

The effects of TiO₂ nanoparticles on the protein expression in mouse lung

Yu-Mi Jeon¹, Seul-Ki Park¹, Wan-Jong Kim², Joo-Hyun Ham³ & Mi-Young Lee^{1,*}

Received: 17 January 2011 / Accepted: 31 May 2011

©The Korean Society of Toxicogenomics and Toxicoproteomics and Springer 2011

Abstract In this study, the differentially expressed proteins by titanium dioxide nanoparticles (TiO₂ NPs) in mouse lung were examined via proteomic approach to better understand the molecular mechanism by which TiO₂ NPs could induce toxicities at the protein level. We identified eight proteins that exhibited more than two-fold changes in expression by TiO₂ NPs. Of these, five proteins, named cytoplasmic aconitase, L-lactate dehydrogenase A chain, carbonic anhydrase 1, pyruvate kinase isoform M2 and peroxiredoxin 6 displayed increased intensities in TiO₂ NP-exposed lungs, while three proteins, named heat shock protein, moesin and apolipoprotein A-1 precursor, showed reduced intensities.

Keywords Proteomics, Mouse, Lung, TiO₂ nanoparticles, Protein expression

Titanium dioxide nanoparticles (TiO₂ NPs) have been widely used in the production of everyday products, such as sunscreens, toothpastes, paper, cosmetics and foods because they have been generally accepted to be of low risk to human health due to their chemical and thermal stability. However, recent studies have reported that exposure to TiO₂ NPs produces various pulmonary effects, including cytotoxicity, oxidative stress, inflammation, proliferation, and histopathologi-

cal responses¹. Moreover, TiO₂ NPs were found to increase the production of hydrogen peroxide and nitric oxide in human bronchial epithelial cells². TiO₂ NP-induced cytotoxicity and reactive oxygen species (ROS) generation caused oxidative DNA damage and mutations, resulting in loss of cell cycle control, cell death, and proliferative disorders³. Numbers of neutrophils and phagocytes in BAL fluid in mice, rats, and hamsters were also elevated by TiO₂ NPs^{4,5}.

Recently, the cytotoxicity of TiO₂ NPs was found to depend not only on particle size, but also on additional factors, such as surface properties, including charge and particle shape. Moreover, in 2006, TiO₂ NPs were classified as a Group 2B carcinogen (possibly carcinogenic to humans) by the International Agency for Research on Cancer (IARC)⁶.

Despite this research, the molecular and cellular mechanism underlying the development of lung tumors in humans and model animals exposed to TiO₂ NPs⁷ remains largely unclear. Moreover, no information regarding the molecular mechanisms by which TiO₂ NPs induce serious toxicity in the lung at the protein level is available. In the present investigation, proteins the expression of which was altered by TiO₂ NPs were identified to better understand the molecular toxicity of TiO₂ NPs at the protein level. Light and transmission electron microscopy were also used to examine the uptake and distribution of TiO₂ NPs in the mouse lung.

Characterization of TiO₂ nanoparticles

Dynamic light scattering (DLS) was used to determine the size distribution of TiO₂ NPs in phosphate-buffered saline (PBS). DLS observations showed that the primary particles (25 nm) in fact showed a wide range of sizes (14.7–631 nm) due to aggregation and agglomera-

¹Department of Medical Biotechnology, Soonchunhyang University, Asan 336-745, Korea

²Department of Life Science, Soonchunhyang University, Asan 336-745, Korea

³Department of Health Management, Hanseo University, Seosan 360-706, Korea

Correspondence and requests for materials should be addressed to M. Y. Lee (✉ miyoung@sch.ac.kr)

tion. The average size was 523.4 ± 95 nm and their hydrodynamic diameter immediately after they were suspended in PBS was 428.95 nm (Table 1). The sizes of the TiO₂ NPs were similar to those of other nanoparticles in PBS and cell culture media⁸.

Table 1. Average size and high distribution of 25-nm anatase TiO₂ nanoparticles in PBS suspension, as measured by DLS analysis.

Diameter (nm)	
Average	High distribution
523.4 ± 95.0	428.95

Microscopic observations

To evaluate the uptake and accumulation of TiO₂ NPs by lung cells, we determined the intracellular localization of TiO₂ NPs by microscopy. TiO₂ NPs were found to form aggregates or agglomerates in the lung. Light microscopic analysis revealed the alveoli to be polyhedral or hexagonal and tightly packed against each other. Each alveolus was lined by squamous epithelium. However, the epithelium lining was noticeably thinner in TiO₂ NPs-exposed lung cells, where TiO₂ NPs accumulated on the surface of the alveoli (Figure 1(A), 1(B)). Additionally, cells lining the alveoli increased in number and had intensely stained nuclei (Figure 1(A), 1(B)).

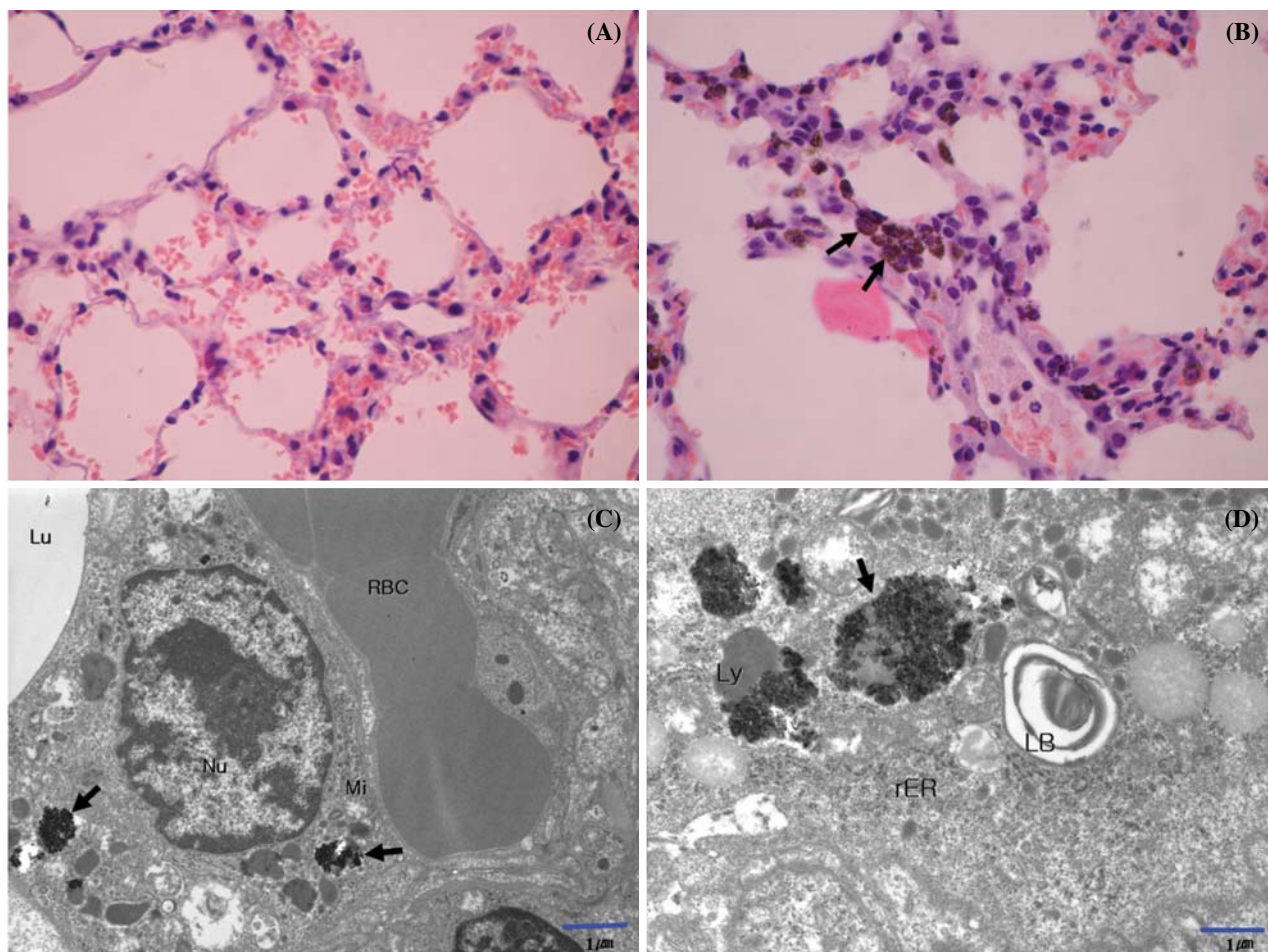


Figure 1. Light and electron microscopic analysis of TiO₂ NP uptake and accumulation. (A) Control mouse lung tissue section showing typical alveoli and interalveolar septa (H&E stain, $\times 400$). (B) Lung section from a TiO₂ NP-exposed mouse showing the precipitation of TiO₂ NPs in the interalveolar septa (H&E stain, $\times 400$). (C) Transmission electron micrograph of cuboidal secretory cells in the lung of a TiO₂ NP-exposed mouse. Lu, alveolar lumen; RBC, red blood cell in a pulmonary capillary, Nu, cell nucleus. Arrows identify TiO₂ NP aggregates. Scale bar=1 μ m. (D) Transmission electron micrograph of part of a macrophage in the lung of a TiO₂ NP-exposed mouse. TiO₂ NPs are clearly distributed within or in close proximity to lysosomes. LB, lamellar body; Ly, lysosome; Mi, mitochondrion; rER, rough endoplasmic reticulum. Arrows identify lysosome-associated TiO₂ NP aggregates. Scale bar=1 μ m.

Electron microscopic analysis showed that the alveolar epithelium consisted largely of simple squamous epithelial cells (type I alveolar cells), with smaller numbers of cuboidal secretory cells (type II alveolar cells). A basket-like network of pulmonary capillaries surrounded each alveolus. Macrophages, which represent an important line of defense, were present within the air space. Precipitated TiO₂ NPs were clearly observed in the alveolar ducts and alveoli of TiO₂ NP-exposed animals. Moreover, particles were accumulated in the cytoplasm of lung macrophages. Many particles were found to localize in lysosomes (Figure 1(C), 1(D)). Some secondary lysosomes and residual bodies were also observed in the cytoplasm (Figure 1(C), 1(D)).

Proteomic analysis of the effects of TiO₂ NPs on protein expression

Two-dimensional gel electrophoresis (2-DE) and MS/MS were used to assess the effects of TiO₂ NPs on lung protein expression. Figure 2 shows 2-DE images of mouse lung proteins following exposure to TiO₂ NPs. More than 870 proteins with isoelectric points (pIs) ranging between 3 and 10 and with relative molecular masses ranging between 6.5 and 205 kDa were detected by 2-DE. After comparing 2-DE protein patterns on duplicate gels, we identified eight protein spots that showed more than two-fold differences in intensity between control and TiO₂ NP-exposed lung samples (Table 2). Of these, five displayed increased intensities in TiO₂ NP-exposed lungs and three, reduced intensities (Figure 2B). The up-regulated proteins were identified by MS/MS as cytoplasmic aconitase, L-lactate dehydrogenase A chain, carbonic anhydrase 1, pyruvate kinase isoform M2, and peroxiredoxin 6, and the down-regulated proteins were heat shock protein 84b, moesin, and apolipoprotein A-1 precursor.

Discussion

Recently, differences in particle dispersion, aggregation

and agglomeration, and in target cell type, were reported to be important determinants of intracellular responses, the degree of cytotoxicity, and potential toxicity mechanisms relating to nanoparticles. The propensity of nanoparticles to agglomerate and aggregate in solution has been known to vary according to ionic strength, temperature, and pH, which may have implications for their uptake into organisms⁹. We characterized TiO₂ NPs by DLS analysis (Table 1). Upon addition to PBS, the 25-nm particles aggregated extensively, such that their mean hydrodynamic diameter, estimated by DLS, was, in fact, 428.95 nm, considerably greater than the primary particle size.

Exposure of mice to TiO₂ NPs resulted in their uptake and accumulation in the lung (Figure 1). TiO₂ NP aggregates were clearly observed in the alveolar duct and alveoli. Light microscopy revealed that the number of cells lining the alveoli increased and the cells had intensely stained nuclei. Moreover, neutrophilic infiltrates surrounded the TiO₂ NP aggregates. Subsequent electron microscopy revealed TiO₂ NP aggregates in the cytoplasm of secretory cells and lung macrophages. Some secondary lysosomes and residual bodies were also observed in the cytoplasm of lung cells in TiO₂ NP-exposed mice. These findings suggest that the accumulation of TiO₂ NPs may represent a non-specific defense mechanism against TiO₂ NPs. Morphologically, hyperplastic epithelial changes were observed in proximity to aggregates of inflammatory cells and particle-laden cells in TiO₂ NP-exposed mice.

We also used proteomic techniques to identify proteins the expression of which in the mouse lung was altered after TiO₂ NP exposure. As a result, eight protein spots displaying greater than two-fold differences in intensity between control and TiO₂ NP-exposed lung samples were identified. Of them, five were up-regulated in TiO₂ NP-exposed mice and the remaining three, down-regulated (Table 2).

Levels of aconitase, an enzyme that catalyzes the interconversion of the anions of three tricarboxylic acids, increased in response to TiO₂ NPs exposure. Aconitase has been shown to be particularly sensitive

Table 2. Proteins, the expression of which was altered in the mouse lung following TiO₂ nanoparticle exposure, identified by LC-MS/MS.

No.	Identified protein	Annotation	Score	Cov %	MW	Change
1	Heat shock protein 84b	IPI00229080.7	218.30	36.05	83280.7	↘
2	Cytoplasmic aconitase	IPI00622780.1	190.29	31.59	99102.0	↗
3	Moesin	IPI00110588.4	70.29	17.16	67766.5	↘
4	Isoform M2 of Pyruvate kinase isozymes M1/M2	IPI00407130.4	230.31	45.76	57844.6	↗
5	L-lactate dehydrogenase A chain	IPI00319994.6	146.30	43.67	36498.3	↗
6	Carbonic anhydrase 1	IPI00230320.6	90.25	47.51	28320.3	↗
7	Apolipoprotein A-I precursor	IPI00121209.1	148.22	49.24	24870.5	↘
8	Peroxiredoxin-6	IPI00555059.2	60.33	32.59	24870.5	↗

↗: Up-regulation, ↘: Down-regulation

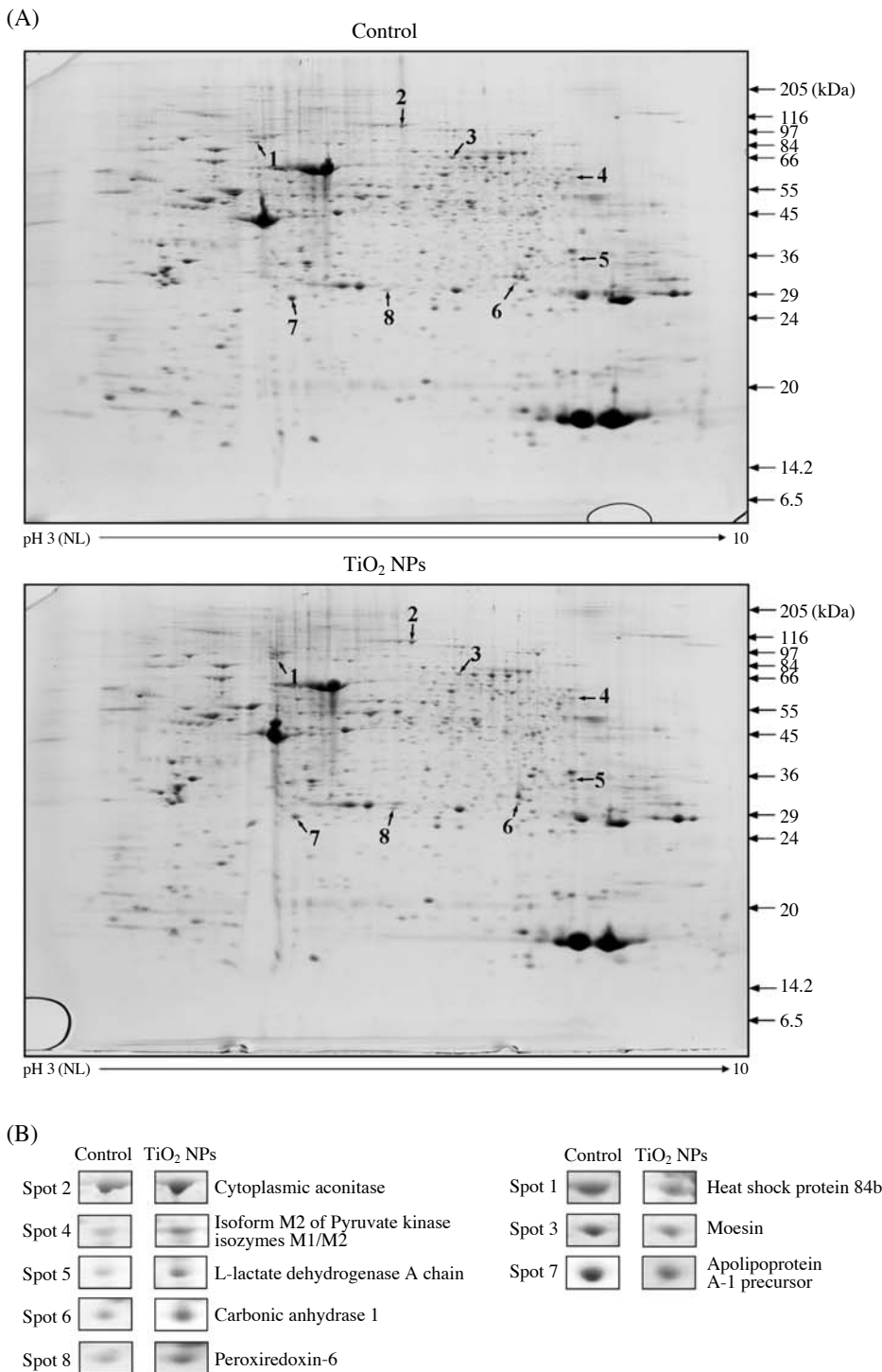
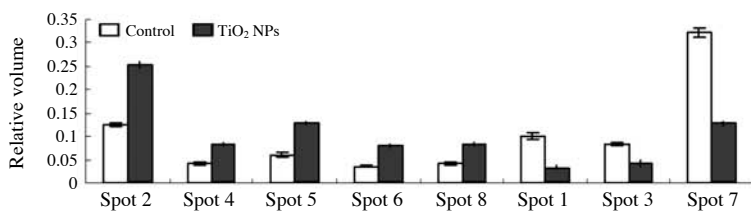


Figure 2. Representative images of mouse lung proteins separated by two-dimensional gel electrophoresis. (A) Proteins on 2-DE gels (pH 3-10) were visualized by Coomassie Brilliant Blue staining. (B) Proteins the expression of which in mouse lung was up- or down-regulated following exposure to TiO₂ NPs. Protein expression levels were determined by measuring relative intensities using image analysis software.



to damage by superoxide anion radicals, while a decrease in its catalytic activity led to the accumulation of ROS¹⁰.

Pyruvate kinase is a well-characterized glycolytic enzyme that catalyzes the conversion of phosphoenol pyruvate to pyruvate, thereby generating ATP from ADP¹¹. It exists as two isozymes, M1 and M2, the latter of which is necessary for aerobic glycolysis in tumor cells and is often used as a cancer biomarker¹². Indeed, the expression of pyruvate kinase M2 has long been known to be elevated in various tumors and it is considered to be a useful biomarker for lung cancer detection¹³. The isozyme of pyruvate kinase that was up-regulated by TiO₂ NPs in the present study may have been M2.

Lactate dehydrogenase (LDH), which catalyses the conversion of lactate to pyruvate, contributes to energy production in cells. A recent report showed that LDH could be used as a prognostic indicator of survival time in terminal cancer patients¹⁴. Elevated LDH were associated with poor survival in lung cancer, pancreatic cancer, colorectal cancer, prostate cancer and hematologic malignancies¹⁴. L-lactate dehydrogenase A chain was up-regulated in the TiO₂ NPs-exposed mouse lung.

To protect against the harmful consequences of oxidative stress, cells express a number of antioxidant enzymes. Peroxiredoxins are a ubiquitous family of antioxidant enzymes that control cytokine-induced peroxide levels and thereby mediate signal transduction in mammalian cells. Peroxiredoxin 6 has been reported to increase lung injury and mouse mortality associated with hypoxia and exposure to paraquat¹⁵. The up-regulation of lung peroxiredoxin 6 levels by TiO₂ NPs may thus play a role in the defense against the toxic effects of TiO₂ NPs.

The expression of carbonic anhydrase 1 was increased following exposure to TiO₂ NPs. Carbonic anhydrases catalyze the rapid conversion of carbon dioxide to bicarbonate and protons, a reaction that occurs rather slowly in the absence of a catalyst¹⁶. They have been shown to be involved in the reduction in tissue pH that is associated with inflammatory pain, and the control of extracellular pH in muscle¹⁷.

Apolipoprotein A-1 (Apo A-1) is the major protein component of high-density lipoprotein (HDL). It has been suggested that Apo A-1 is a potent inhibitor of inflammation¹⁸. In support of this, it was shown to block T cell signals from macrophages and to inhibit the production of tumor necrosis factor alpha (TNF- α) and interleukin-1¹⁹. The marked decrease in Apo A-1 precursor levels in the present study suggests that TiO₂ NPs may cause lung inflammation.

Moesin is a member of the ezrin/radixin/moesin (ERM) protein family. ERM proteins act as membrane-

cytoskeleton linkers in actin-enriched specialized membrane structures named microvilli, ruffles, and cleavage furrows. They appear to play roles in the control of cell morphology, adhesion, and motility²⁰. Notably, moesin is important for cell-cell recognition and signaling and cell movement. The results of one experiment have linked moesin to tumor biology, showing its expression to be associated with papillary thyroid carcinomas, oral squamous cell carcinomas, and basal breast carcinomas²⁰. Decreased moesin expression in TiO₂ NP-exposed mice in the present study may thus reflect lung cell dysfunction or transformation.

Heat shock proteins are key molecular chaperones that stabilize proteins, refold misfolded proteins, and target irreversibly damaged proteins for degradation. Additionally, they regulate cell proliferation, cell cycle, and apoptotic pathways, and have been implicated in multiple pathologies²¹. Some of the most abundant cytosolic molecular chaperones, heat shock proteins, have emerged as promising anticancer targets²². In the present study, heat shock protein 84b was down-regulated in the lungs of TiO₂ NP-exposed mice, suggesting the possible induction of apoptosis²².

In this study, the obvious accumulation of TiO₂ NPs in the lung was associated with local histopathological changes, including alveolar septal thickening, neutrophil infiltration, and hyperplastic epithelial changes. Collectively, these changes probably resulted in lung function being impaired. Moreover, the expression of cancer-related proteins (pyruvate kinase, L-lactate dehydrogenase A chain, moesin and heat shock protein 84b), oxidative stress-linked proteins (peroxiredoxin 6 and cytoplasmic aconitase), and inflammation-associated proteins (carbonic anhydrase 1 and apolipoprotein A-1 precursors) were shown to be altered following exposure to TiO₂ NPs. The identification of these proteins may offer insights into the mechanisms behind TiO₂ NP-induced toxicity. The proteins themselves could potentially be used as biomarkers for the prediction and diagnosis of TiO₂ NP-induced pulmonary toxicity.

Materials & Methods

Dynamic light scattering analysis

The average sizes of 25-nm TiO₂ NP aggregates or agglomerates in aqueous solutions were determined by dynamic light scattering (DLS). TiO₂ NPs were suspended in phosphate-buffered saline (PBS) at a concentration of 1 mg/mL, shaken, and dispersed by ultrasonic vibration for 10 min. The suspension was then characterized through DLS at a wavelength of 659 nm and with a detection angle of 90°, performed

using a Zetasizer-3000 particle size analyzer²³.

Experimental animals

Male ICR mice (7-weeks-old, weighing 18 ± 2 g) were purchased from Orient Bio Co. Ltd. (Seoul, Korea). Room temperature was maintained at $20 \pm 2^\circ\text{C}$ and the relative humidity at $60 \pm 10\%$. The mice were exposed to a normal day/night cycle prior to the start of the experiment. They were fed on water and sterilized food.

Commercial TiO_2 NPs (Sigma-Aldrich), composed of the crystallographic form of TiO_2 (anatase) with an average diameter of < 25 nm, were mixed with PBS. The suspension was then ultrasonicated for 10 min in a sealed sterile tube.

Male ICR mice were randomly assigned to control and treatment groups ($n=6$). Animals in the treatment group were injected intraperitoneally (i.p.) with 2.5 mg of TiO_2 NPs suspended in 0.2 mL of endotoxin-free PBS. At 30 min post-injection, 100 μL of TiO_2 NP suspension was instilled nasally every day for 7 days. After 7 days, all animals were anaesthetized with ether and sacrificed, and their lungs were harvested and stored at -70°C .

Preparation of protein extracts for 2-DE

Lung tissues were snap frozen in liquid N_2 and stored at -70°C until analysis. Frozen lung tissue samples (100 mg) were homogenized in rehydration buffer (7 M urea, 2 M thiourea, 4.5% (w/v) CHAPS, 40 mM Tris, 100 mM DTE, 0.25% IPG buffer (pH 3-10)) containing a protease inhibitor cocktail. Solubilized tissue was centrifuged (12,000 g, 30 min, 4°C) and the resulting supernatant fractions were analyzed by two-dimensional gel electrophoresis^{24,25}.

Two-dimensional gel electrophoresis

Isoelectric focusing (IEF) was carried out using immobilized pH gradient (IPG) strips (24 cm, pH 3-10; ImmobilineTM DryStrip; GE Healthcare Biosciences)²⁶. Protein (1 mg) was mixed with rehydration buffer and loaded onto first-dimension IPG strips and focused through electrophoresis for a total of 84 kVh at 20°C . Focusing was performed through the following steps: rehydration for 12 h, 200 V/200 Vh, 500 V/500 Vh, 1,000 V/1,000 Vh, 8,000 V/13,500 Vh, and 8,000 V/100,000 Vh. After isoelectric focusing, the strips were twice soaked for 20 min in equilibration buffer (6 M urea, 2% (w/v) SDS, 20% (v/v) glycerol, 5 mM tributylphosphine, 2.5% acrylamide, 0.01% bromophenol blue, 0.375 M Tris-HCl, pH 8.8). The second-dimension separation, SDS-PAGE, was performed using 8-16% gradient polyacrylamide gels without stacking gels.

Proteins were separated by electrophoresis at 10°C for 2 h at 5 mA/gel and then at 18 mA/gel. Electrophoresis was stopped when the dye front began to diffuse from the gel.

Protein identification by LC-MS/MS

The spots of interest were excised from the 2-DE gels, destained, dried, and in-gel digested for 2 h at 37°C in a solution containing both trypsin and a protease mixture. An electrospray ionization trap mass spectrometer (LCQ Deca XP; Thermo Finnigan) was used for peptide detection. The positive ion mode was selected and the spray voltage set to 2.5 kV. The spray temperature for analyzing peptides was set to 150°C . In LC-MS/MS mode, the mass spectrometer automatically set the collision energy. After acquisition of full-scan mass spectra, three LC-MS/MS scans for the next most intense ions were acquired through dynamic exclusion. All product ions were used in a computer database search performed using the Mascot MS/MS ion search tool from the NCBI database (NIH, Bethesda MD, USA).

Light microscopy (LM)

Small pieces of lung were excised and immediately fixed in a 10% formalin solution. Tissues were embedded in paraffin blocks, sectioned at 5 μm , and attached to glass slides. They were then subjected to hematoxylin and eosin staining, and analyzed by a pathologist blinded to the experiment²⁷.

Transmission electron microscopy (TEM)

Pieces of lung tissue were removed from each animal and immersed in 3% glutaraldehyde for 3 h. They were then washed in Millonig's phosphate buffer and post-fixed in 1% osmium tetroxide (OsO_4) for 3 h. After fixation, the tissues were dehydrated through a graded series of ethanol solutions, treated with propylene oxide for 30 min, and embedded in a graded araldite mixture. For ultrastructural analysis, serial ultrathin sections (100 nm) were cut using a DuPont diamond knife. Sections were collected onto copper grids and stained with uranyl acetate followed by lead citrate. The ultrastructures of the stained sections were examined using a JEOL-1010 transmission electron microscope²⁸.

References

1. Park, E. J., Yoon, J., Choi, K., Yi, J. & Park, K. S. Induction of chronic inflammation in mice treated with titanium dioxide nanoparticles by intratracheal instilla-

- tion. *Toxicology* **260**:37-46 (2009).
2. Gurr, J. R., Wang, A. S., Chen, C. H. & Jan, K. Y. Ultrafine titanium dioxide particles in the absence of photoactivation can induce oxidative damage to human bronchial epithelial cells. *Toxicology* **213**:66-73 (2005).
 3. Kim, Y. J. *et al.* Genotoxicity of aluminum oxide (Al₂O₃) nanoparticle in mammalian cell lines. *Mol Cell Toxicol* **5**:172-178 (2009).
 4. Chen, H. W. *et al.* Titanium dioxide nanoparticles induce emphysema-like lung injury in mice. *FASEB J* **20**:2393-2395 (2006).
 5. Wang, J. *et al.* Acute toxicity and biodistribution of different sized titanium dioxide particles in mice after oral administration. *Toxicol Lett* **168**:176-185 (2007).
 6. Xu, J. *et al.* Involvement of macrophage inflammatory protein 1alpha (MIP 1 alpha) in promotion of rat lung and mammary carcinogenic activity of nanoscale titanium dioxide particles administered by intra-pulmonary spraying. *Carcinogenesis* **31**:927-935 (2010).
 7. Linnainmaa, K., Kivipensas, P. & Vainio, H. Toxicity and cytogenetic studies of ultrafine titanium dioxide in cultured rat liver epithelial cells. *Toxicol In Vitro* **11**:329-335 (1997).
 8. Sohaebuddin, S. K., Thevenot, P. T., Baker, D., Eaton, J. W. & Tang, L. Nanomaterial cytotoxicity is composition, size, and cell type dependent. *Part Fibre Toxicol* **7**:22 (2010).
 9. Scown, T. M. *et al.* High doses of intravenously administered titanium dioxide nanoparticles accumulate in the kidneys of rainbow trout but with no observable impairment of renal function. *Toxicol Sci* **109**: 372-380 (2009).
 10. Qin, G., Meng, X., Wang, Q. & Tian, S. Oxidative damage of mitochondrial proteins contributes to fruit senescence: a redox proteomics analysis. *J Proteome Res* **8**:2449-2462 (2009).
 11. DeSouza, L. V. *et al.* Multiple reaction monitoring of mTRAQ-labeled peptides enables absolute quantification of endogenous levels of a potential cancer marker in cancerous and normal endometrial tissues. *J Proteome Res* **7**:3525-3534 (2008).
 12. Christofk, H. R., Vander Heiden, M. G., Wu, N., Asara, J. M. & Cantley, L. C. Pyruvate kinase M2 is a phosphotyrosine-binding protein. *Nature* **452**:181-186 (2008).
 13. Schneider, J., Morr, H., Velcovsky, H. G., Weisse, G. & Eigenbrodt, E. Quantitative detection of tumor M2-pyruvate kinase in plasma of patients with lung cancer in comparison to other lung diseases. *Cancer Detect Prev* **24**:531-535 (2000).
 14. Suh, S. Y. & Ahn, H. Y. Lactate dehydrogenase as a prognostic factor for survival time of terminally ill cancer patients: a preliminary study. *Eur J Cancer* **43**:1051-1059 (2007).
 15. Wang, Y., Feinstein, S. I. & Fisher, A. B. Peroxiredoxin 6 as an antioxidant enzyme: protection of lung alveolar epithelial type II cells from H₂O₂-induced oxidative stress. *J Cell Biochem* **104**:1274-1285 (2008).
 16. Badger, M. R. & Price, G. D. The role of carbonic anhydrase in photosynthesis. *Ann Rev Plant Physiol Plant Mol Biol* **45**:369-392 (1994).
 17. Radhakrishnan, R. & Sluka, K. A. Acetazolamide, a carbonic anhydrase inhibitor, reverses inflammation-induced thermal hyperalgesia in rats. *J Pharmacol Exp Ther* **313**:921-927 (2005).
 18. Vuilleumier, N. *et al.* Presence of autoantibodies to apolipoprotein A-1 in patients with acute coronary syndrome further links autoimmunity to cardiovascular disease. *J Autoimmun* **23**:353-360 (2004).
 19. Hyka, N. *et al.* Apolipoprotein A-1 inhibits the production of interleukin-1beta and tumor necrosis factor-alpha by blocking contact-mediated activation of monocytes by T lymphocytes. *Blood* **97**:2381-2389 (2001).
 20. Charafe-Jauffret, E. *et al.* Moesin expression is a marker of basal breast carcinomas. *Int J Cancer* **121**: 1779-1785 (2007).
 21. Blackford, J. A. Jr., Jones, W., Dey, R. D. & Castranova, V. Comparison of inducible nitric oxide synthase gene expression and lung inflammation following intratracheal instillation of silica, coal, carbonyl iron, or titanium dioxide in rats. *J Toxicol Environ Health* **51**:203-218 (1997).
 22. Taiyab, A., Sreedhar, A. S. & Rao, Ch. M. Hsp90 inhibitors, GA and 17AAG, lead to ER stress-induced apoptosis in rat histiocytoma. *Biochem Pharmacol* **78**:142-152 (2009).
 23. Liu, S., Xu, L., Zhang, T., Ren, G. & Yang, Z. Oxidative stress and apoptosis induced by nanosized titanium dioxide in PC12 cells. *Toxicology* **267**:172-177 (2010).
 24. Park, S. K., Nam, S. W. & Lee, M. Y. Ethylbenzene-induced differential protein profiles in rat liver. *BioChip J* **4**:272-278 (2010).
 25. Jeon, Y. M., Park, S. K., Rhee, S. K. & Lee, M. Y. Proteomic profiling of the differentially expressed proteins by TiO₂ nanoparticles in mouse kidney. *Mol Cell Toxicol* **6**:419-425 (2010).
 26. Park, S. K., Jeon, Y. M., Son, B. S., Youn, H. S. & Lee, M. Y. Proteomic analysis of the differentially expressed proteins by airborne nanoparticles. *J Appl Toxicol* **31**:463-470 (2011).
 27. Lee, S. E. *et al.* Systemic immunity of obese-diabetes model (*db/db*) mice. *Mol Cell Toxicol* **6**:143-149 (2010).
 28. Al-Banna, N. A., Junaid, T. A., Mathew, T. C., Raghupathy, R. & Albert, M. J. Histopathological and ultrastructural studies of a mouse lung model of *Campylobacter jejuni* infection. *J Med Microbiol* **57**:210-217 (2008).